

Electron-nuclear spin dynamics of Ga²⁺ paramagnetic centers probed by spin-dependent recombination: A master equation approach

V. G. Ibarra-Sierra,¹ J. C. Sandoval-Santana,¹ S. Azaizia,² H. Carrère,² L. A. Bakaleinikov,³ V. K. Kalevich,³ E. L. Ivchenko,³ X. Marie,² T. Amand,² A. Balocchi,² and A. Kunold⁴

¹*Departamento de Física, Universidad Autónoma Metropolitana Iztapalapa, Av. San Rafael Atlixco 186, Col. Vicentina, 09340 Ciudad de México, Mexico*

²*Université de Toulouse, INSA-CNRS-UPS, LPCNO, 135 avenue de Rangueil, 31077 Toulouse, France*

³*Ioffe Physical-Technical Institute, 194021 St. Petersburg, Russia*

⁴*Área de Física Teórica y Materia Condensada, Universidad Autónoma Metropolitana Azcapotzalco, Av. San Pablo 180, Col. Reynosa-Tamaulipas, 02200 Ciudad de México, Mexico*

(Received 13 November 2016; revised manuscript received 3 April 2017; published 10 May 2017)

Similar to nitrogen-vacancy centers in diamond and impurity atoms in silicon, interstitial gallium deep paramagnetic centers in GaAsN have been proven to have useful characteristics for the development of spintronic devices. Among other interesting properties, under circularly polarized light, gallium centers act as spin filters that dynamically polarize free and bound electrons reaching record spin polarizations (close to 100%). Furthermore, the recent observation of the amplification of the spin filtering effect under a Faraday configuration magnetic field has suggested that the hyperfine interaction that couples bound electrons and nuclei permits the optical manipulation of the nuclear spin polarization. Even though the mechanisms behind the nuclear spin polarization in gallium centers are fairly well understood, the origin of nuclear spin relaxation and the formation of an Overhauser-like magnetic field remain elusive. In this work we develop a model based on the master equation approach to describe the evolution of electronic and nuclear spin polarizations of gallium centers interacting with free electrons and holes. Our results are in good agreement with existing experimental observations. In particular, we are able to reproduce the amplification of the spin filtering effect under a circularly polarized excitation in a Faraday configuration magnetic field. In regard to the nuclear spin relaxation, the roles of nuclear dipolar and quadrupolar interactions are discussed. Our findings show that, besides the hyperfine interaction, the spin relaxation mechanisms are key to understand the amplification of the spin filtering effect and the appearance of the Overhauser-like magnetic field. To gain a deeper insight in the interplay of the hyperfine interaction and the relaxation mechanisms, we have also performed calculations in the pulsed excitation regime. Our model's results allow us to propose an experimental protocol based on time-resolved spectroscopy. It consists of a pump-probe photoluminescence scheme with the detection and the tracing of the electron-nucleus flip-flops through photoluminescence measurements.

DOI: [10.1103/PhysRevB.95.195204](https://doi.org/10.1103/PhysRevB.95.195204)

I. INTRODUCTION

Negatively charged nitrogen-vacancy centers in diamond [1–5], phosphorous atom impurities in silicon [6–11], and other schemes based on point defects embedded in semiconductors have been widely studied as alternatives to develop quantum bits [12,13]. One of the necessary conditions for quantum computing is long electron spin decoherence times to ensure a minimum of fault tolerance [10,14]. In diamond's nitrogen-vacancy centers [15], silicon vacancies in silicon carbide [16], silicon [17], and any III-V based quantum dots [10,18] the fluctuating nuclear bath is the main source limiting spin coherence time. The nuclear dipole-dipole interaction is believed to be the dominant mechanism behind the diffusion-induced electron-spin decoherence [19]. To protect the dynamics of the nuclear spins of point defects from the decoherence induced by the environment, semiconductors mainly composed of spin-zero isotopes such as silicon and carbon are preferred over III-V semiconductors [5]. Even though the two stable isotopes of Ga, ⁶⁹Ga and ⁷¹Ga, have nuclear spin 3/2, in dilute nitride GaAsN point interstitial defects give rise to paramagnetic centers that have very peculiar and useful properties. One of them is the spin-dependent recombination (SDR) [20–27]. In Ga(In)NAs

alloys, Ga_i²⁺ paramagnetic centers with only one bound electron can selectively capture another conduction band (CB) electron with the opposite spin orientation [26–30]. Due to this mechanism, paramagnetic centers act as a spin filter that blocks the recombination of CB electrons with the same spin and efficiently captures electrons whose spin is in the opposite direction. In the centers, the bound and captured electrons form a singlet state that is destroyed as either one of the electrons recombines to the valence band (VB). It is important to note that while the lifetime of conduction electrons with the spin opposite to that of the bound electrons is a few picoseconds, the lifetime of conduction electrons copolarized with the majority of bound electrons may extend to nanoseconds. As a consequence the free photoelectron spin polarization can reach over 80% under circularly polarized incident light. Additionally the photoluminescence (PL) intensity can be as high as 800% under circularly polarized optical excitation compared to a linearly polarized one [21,22]. The increase in CB electron population allows even for the detection of electron spin polarization by electrical means due to a giant photoconductivity effect under circularly polarized light [24,31].

Whereas in diamond and silicon the optical excitation acts directly on the point defects, in GaAsN the bound electron is

dynamically spin polarized due to the recombination of spin-polarized CB electrons on the paramagnetic centers. Although this mechanism is radically different, Ga_i^{2+} centers themselves are very similar to nitrogen vacancies and phosphorous atoms. Recent experiments on GaAsN subject to a weak magnetic field in Faraday configuration [32–35] have shown consistently an enhancement in the spin-filtering mechanism in comparison to the zero magnetic field. The general agreement among different models [28,35–37] is that the hyperfine interaction between the bound electron and the nucleus in the centers is the key element behind this phenomenon. At low magnetic fields, the spin-filtering effect is reduced due to spin-state mixing induced by the hyperfine interaction. For higher values of the magnetic field such that the Zeeman energy exceeds the hyperfine interaction, the pure bound electron spin states and, consequently, the spin-filtering effect are recovered. Even though the role of the hyperfine interaction is well established, some aspects of these phenomena lack full understanding. Some observations point to the existence of an Overhauser-like effective magnetic field [32,33] whose origin is yet unclear. It manifests as a shift in the band to band PL intensity or the degree of CB electron spin polarization as functions of the longitudinal magnetic field. These two curves shift to the positive or negative regions of the magnetic field depending on the helicity of the circularly polarized light. Another aspect that needs further study is the nuclear interaction between Ga_i^{2+} centers and adjacent Ga atoms that would lead to nuclear spin relaxation. The Overhauser-like magnetic field has been correctly reproduced in Ref. [36], however, nuclear spins are assumed to relax very rapidly and the relaxation mechanism is purely phenomenological. Moreover, when a trap captures an electron it is assumed to instantly lose all its nuclear spin polarization. On the other hand, the model presented in Ref. [37] considers two phenomenological and arbitrary nuclear spin relaxation times for traps with one and two bound electrons. Despite this improvement, the model considers Ga centers with 1/2 nuclear spins instead of 3/2 in order to simplify the kinetic equations. Even though the first version of this model can only address experimental conditions in which the magnetic field is in Faraday configuration, it was later generalized to consider tilted magnetic fields by introducing off-diagonal terms [38]. However, this model is strictly valid for Ga paramagnetic traps with 1/2 nuclear spins. Although the SDR mechanisms are partially integrated to the rate equation approach [35], the off-diagonal elements of the master equation are neglected and therefore the hyperfine interaction is accounted for by phenomenological transition rates. This analysis has two major limitations: first, it only allows for the study of situations in which the magnetic field is in Faraday configuration and, second, it does not take into account the full complexity of the hyperfine interaction off-diagonal terms. Even though this analysis gives the correct behavior for the conduction band electron spin polarization degree as function of the longitudinal magnetic field, it fails to explain the origin of the Overhauser-like effective field. It considers that the Overhauser-like field is proportional to the nuclear degree of polarization regardless of the nuclear spin. This contradicts the fact that for 1/2 nuclear spins the magnetic field shift is strictly zero even for nuclear spin polarization degrees close to 100% [37].

In this paper we examine the spin dynamics in GaAsN alloys. We propose a model based on the master equation for the density matrix that describes the main interactions between CB electrons, VB holes, and paramagnetic traps. Our approach overcomes most of the limitations of the previous models. First, it considers Ga centers with 3/2 nuclear spin. Second, in contrast to older proposals, all of the off-diagonal elements arising from the preexisting two-charge model [20,21,27,29,39], are taken into account. This introduces the main mechanisms of SDR into the model. The major advantage of this improvement is that it can be used to study experimental conditions in which the magnetic field is tilted with respect to the incident light. Finally, the spin relaxation mechanism was introduced through Wangsness, Bloch, and Redfield relaxation theory [40–43]. Two interactions are explored as possible candidates to produce the nuclear spin relaxation: dipolar interaction between neighboring nuclei [40] and quadrupolar [40,44] interaction with charge fluctuations in the environment. This not only has allowed us to clearly identify the dipolar interaction as the dominant nuclear relaxation mechanism but has also shown that the Overhauser-like magnetic field originates from it.

To further explore the role of hyperfine interaction in Ga centers, we have studied the time-resolved electronic and nuclear spin polarizations under pulsed excitation. Using these results we outline a method based on a pump-probe photoluminescence scheme to trace the coherent evolution of coupled electron and nuclear spins as they flip-flop due to the hyperfine interaction.

This paper is organized as follows. In Sec. II we introduce the master equation model that describes the key processes in the spin dynamics of electrons and nuclei in GaAsN. The role of the hyperfine interaction and the nuclear spin relaxation mechanism are discussed in this section. The mathematical forms of the dipolar and quadrupolar dissipators are introduced in Sec. II D. In Sec. III A we establish the main mechanism behind the nuclear spin relaxation in Ga^{2+} centers by comparing the theoretical results issued by the model with existing experimental results. Simulations in the pulsed excitation regime are presented in Sec. III B. In Sec. IV we summarize the main results.

II. MASTER EQUATION

The system mainly consists of four elements: VB holes, CB electrons, unpaired traps, and paired traps. Whereas hole spin relaxes with a characteristic time below 1 ps [45], CB electronic spin relaxes on a typical time in the range 100–400 ps [25,46]. Therefore, for the sake of simplicity, we consider VB holes to be unpolarized. Gallium paramagnetic traps or unpaired traps can be understood as a 3/2 nuclear spin coupled to a 1/2 bound electron spin via hyperfine interaction. On the other hand, when a CB electron is captured by an unpaired trap, forming a paired trap, the bound and captured electrons produce a singlet state that cannot interact with the nuclear spin. Thus, the quantum state basis that describes this system must have: (i) one state for holes in the VB; (ii) two states for the spin-up and spin-down CB electrons; (iii) eight states that account for the nucleus-bound electron system in the unpaired traps; and (iv) four states for the nuclear spin in

the paired traps. The complete quantum state basis is therefore given by

$$\begin{aligned} \mathcal{B} = \{ & |1\rangle = |h\rangle, |2\rangle = |\downarrow\rangle, |3\rangle = |\uparrow\rangle, |4\rangle = |-\frac{3}{2}, \downarrow\rangle, \\ & |5\rangle = |-\frac{1}{2}, \downarrow\rangle, |6\rangle = |\frac{1}{2}, \downarrow\rangle, |7\rangle = |\frac{3}{2}, \downarrow\rangle, \\ & |8\rangle = |-\frac{3}{2}, \uparrow\rangle, |9\rangle = |-\frac{1}{2}, \uparrow\rangle, |10\rangle = |\frac{1}{2}, \uparrow\rangle, \\ & |11\rangle = |\frac{3}{2}, \uparrow\rangle, |12\rangle = |-\frac{3}{2}, \uparrow\downarrow\rangle, \\ & |13\rangle = |-\frac{1}{2}, \uparrow\downarrow\rangle, |14\rangle = |\frac{1}{2}, \uparrow\downarrow\rangle, |15\rangle = |\frac{3}{2}, \uparrow\downarrow\rangle \}, \end{aligned} \quad (1)$$

where $|h\rangle$ is the VB hole state and $|\uparrow\rangle$ and $|\downarrow\rangle$ are the spin-up and spin-down CB electron states, respectively. The following eight states $|-\frac{3}{2}, \downarrow\rangle, |-\frac{1}{2}, \downarrow\rangle, \dots, |\frac{3}{2}, \uparrow\rangle$ are the bound-electron and nuclear spin states projected along the z axis corresponding to the unpaired trap. Finally, the paired traps are described by the nuclear spin states $|-\frac{3}{2}, \uparrow\downarrow\rangle, \dots, |\frac{3}{2}, \uparrow\downarrow\rangle$.

The dynamics of the four parts of the system and their interactions can be described through the master equation

$$\frac{d\rho}{dt} = \frac{i}{\hbar}[\rho, H] + \mathcal{D}(\rho), \quad (2)$$

where ρ is the density matrix, H is the Hamiltonian and $\mathcal{D}(\rho)$ is the dissipator. The Hamiltonian contains the internal interactions among the four components of the system. We are interested in the combined effect of an external magnetic field and the hyperfine interaction in Ga centers, therefore, the Hamiltonian must contain Zeeman and hyperfine interaction terms. The interactions among the different parts of the system and the surroundings are accounted for by the dissipator. These are mostly interactions with the electromagnetic field, occurring during recombination or excitation processes, or interactions with the nuclear spin environment. The main processes introduced in our model are schematized in Fig. 1.

A. Hamiltonian: Zeeman and hyperfine interactions

The Hamiltonian is given by

$$H = \hbar\omega \cdot \hat{S} + \hbar\Omega \cdot \hat{S}_c + A\hat{I}_1 \cdot \hat{S}_c. \quad (3)$$

The first and second terms in the Hamiltonian correspond to the Zeeman interaction for conduction and bound electrons, respectively. In these terms $\omega = g\mu_B \mathbf{B}/\hbar$, $\Omega = g_c\mu_B \mathbf{B}/\hbar$, \mathbf{B} is the external magnetic field, μ_B is the Bohr magneton and, g and g_c are the CB and bound electrons gyromagnetic factors. The hyperfine interaction term, the third one on the right-hand side of Eq. (3), couples the bound electron and the nuclear spin in an unpaired trap. The hyperfine coupling constant is given by A . Other possible interactions between the electron spins and the many surrounding nuclear spins are neglected. The strong localization of the $4s$ electrons wave function in Ga centers [47] in the vicinity of the nucleus $|\psi_{4s}|^2 = 72.7 \times 10^{24} \text{ cm}^{-3}$ yields a large hyperfine parameter $A \approx 8.5 \text{ eV}$ coupling bound electrons and the corresponding nuclei. Conversely, CB electrons weakly interact with the surrounding nuclear spins giving their small probability density $|\psi_{CB}|^2 \approx 1/V = 1 \times 10^{13} \text{ cm}^{-3}$, where V is the sample volume. Therefore, the hyperfine interaction between CB electrons and all the surrounding nuclei is neglected. Moreover, the nuclear spin polarization of the host atoms surrounding the defects should be ruled out, because otherwise it would

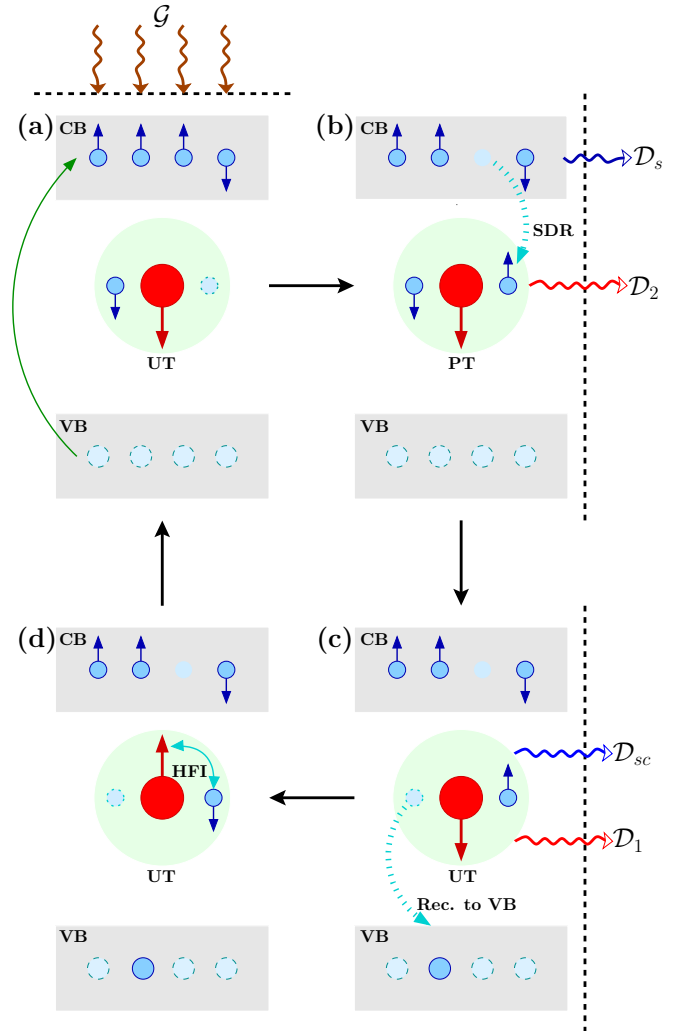


FIG. 1. Schematic diagram of the processes involved in the nuclear spin polarization of Ga centers. The flow of angular momentum is also shown. Following the selection rules for GaAs, three spin-up, one spin-down CB electrons, and four unpolarized VB holes are generated by four photons with 100% left circular polarization (a). The angular momentum of photons is transferred to the CB electrons. Traps whose bound electrons are spin polarized in the opposite direction to the majority of the CB electrons, can capture CB electrons with opposite spin orientation forming a spin singlet (b). In a course of this process the angular momentum of the CB electrons is transferred partly to the bound electrons in traps. Simultaneously, CB electrons' spin and paired traps nuclear spin relax due to \mathcal{D}_S and \mathcal{D}_2 leading to loss of angular momentum by the system. When one of the trapped electrons recombines with the hole the spin singlet in the paired trap is dissociated and turns into an unpaired trap (c). At the same time, the bound electron and nuclear spins in the unpaired trap relax due to the \mathcal{D}_{SC} and \mathcal{D}_1 dissipators (c). Again the system transfers to angular momentum to the environment. At this stage the bound electron and the nucleus are able to interact via the hyperfine interaction and exchange angular momentum through the series of flip-flops (d). From (d) to (a) the center can capture a new electron and the cycle starts again.

cause a noticeable shift of the optically detected electron spin resonance lines, which was not observed in high-resolution experiments [35,47]. The dynamic polarization of the host

nuclei as the source of an Overhauser field must also be excluded from the model. The remarkable signature of such a field is an additional maximum that appears in the Hanle curve and shifts with respect to the zero magnetic field [48–50]. A very recent experiment performed in GaAsN subjected to tilted magnetic fields [38] clearly shows the absence of the additional peak.

The spin operator for CB electrons that appears in the first Zeeman term of the Hamiltonian is $\hat{S} = (\hat{S}_x, \hat{S}_y, \hat{S}_z)$. In unpaired traps, the bound electron spin and nuclear spin operators entering the hyperfine interaction term are $\hat{S}_c = (\hat{S}_{cx}, \hat{S}_{cy}, \hat{S}_{cz})$, and $\hat{I}_1 = (\hat{I}_{1x}, \hat{I}_{1y}, \hat{I}_{1z})$, respectively. As the singlet state formed in the paired traps interacts neither with the external magnetic field nor with their nuclear spin $\hat{I}_2 = (\hat{I}_{2x}, \hat{I}_{2y}, \hat{I}_{2z})$, it does not appear in the Hamiltonian.

B. Density matrix operator space

The relaxation mechanisms of CB electrons and nuclei in the Ga centers are described by the dissipator $\mathcal{D}(\rho)$. Also, the photoexcitation and recombination of electrons will be accounted for by \mathcal{D} .

Our approach to formulating a suitable dissipator consists in expanding the relevant operators as linear combination of the elements of an operator vector space. In principle this set should be formed in the basis (1) by linearly independent 15×15 Hermitian matrices. However, the density matrix structure is considerably simplified by assuming that the four components of the system (CB, unpaired trap, paired trap, VB) are interconnected only by the dissipator. As the four parts of the system are exclusively coupled by the recombination or excitation processes, this is a reasonable assumption. Thus, the density matrix operator can be presented in the block diagonal form:

$$\rho = \begin{pmatrix} \rho_{\text{VB}} & & & \\ & \rho_{\text{CB}} & & \\ & & \rho_1 & \\ & & & \rho_2 \end{pmatrix}, \quad (4)$$

where the four blocks ρ_{VB} (1×1), ρ_{CB} (2×2), ρ_1 (8×8), and ρ_2 (4×4) are the partial density matrices of VB holes, CB electrons, unpaired traps, and paired traps, respectively. Given that ρ takes the form of a block diagonal matrix since no coherences can arise between the four components, it suffices to consider the smaller vector space of 85 Hermitian matrices that generate the four blocks.

We start by finding an internal space of Hermitian matrices

$$\Lambda = \{\hat{\lambda}_1, \hat{\lambda}_2, \dots, \hat{\lambda}_n\}, \quad (5)$$

which spans the $n = 85$ relevant elements of the 15×15 matrix. The generators in this set can be chosen in such a way that they are Hermitian and orthogonal with respect to the scalar product given by the trace

$$\langle \hat{\lambda}_i, \hat{\lambda}_j \rangle \equiv \text{Tr}[\hat{\lambda}_i^\dagger \hat{\lambda}_j] = \delta_{i,j} \text{Tr}[\hat{\lambda}_i^2]. \quad (6)$$

This choice conveniently links the inner product with the expected value of a given operator \hat{O}

$$O = \text{Tr}[\hat{O}\rho] = \langle \rho, \hat{O} \rangle, \quad (7)$$

acting on ρ . In this manner any operator can be expanded as a linear combination of the elements of (5) as

$$\hat{O} = \sum_{q=1}^{85} \frac{\text{Tr}[\hat{\lambda}_q \hat{O}]}{\text{Tr}[\hat{\lambda}_q^2]} \hat{\lambda}_q. \quad (8)$$

A very convenient set of operators is the one formed by the generators of the unitary groups $U(1)$ (VB holes), $U(2)$ (CB electrons), $U(4)$ (paired traps), and $U(8)$ (unpaired traps). The operators forming this set are not only of physical significance but they are also linearly independent and orthogonal with respect to the trace. Explicitly, the set of operators in (5) is given by

$$\Lambda = \{\hat{p}, \hat{S}_i, \hat{U}_{k,j,i}, \hat{T}_{j,i}\}, \quad i, j, k = 0, 1, 2, 3, \quad (9)$$

where \hat{p} , \hat{S}_i , $\hat{U}_{k,j,i}$, and $\hat{T}_{j,i}$ generate the VB, CB, unpaired trap, and paired trap blocks. The VB hole population density operator can be represented by the matrix

$$\hat{p} = \begin{pmatrix} 1 & & & \\ & 0_{2 \times 2} & & \\ & & 0_{8 \times 8} & \\ & & & 0_{4 \times 4} \end{pmatrix}. \quad (10)$$

The operators that generate the CB block can be compiled in the matrix

$$\hat{S}_i = \begin{pmatrix} 0 & & & \\ & \hat{s}_i & & \\ & & 0_{8 \times 8} & \\ & & & 0_{4 \times 4} \end{pmatrix}, \quad i = 0, 1, 2, 3, \quad (11)$$

where the electron population density in the CB is given by $\hat{n} = \hat{S}_0$ and their spin operators are \hat{S}_i for $i = 1, 2, 3$. Here $\hat{s}_0 = \hat{I}_{2 \times 2}$ is the 2×2 identity matrix, and \hat{s}_i for $i = 1, 2, 3$ are the standard Pauli spin matrices that fulfill the usual spin commutation relations

$$[\hat{s}_i, \hat{s}_j] = i \sum_{k=1,2,3} \epsilon_{ijk} \hat{s}_k. \quad (12)$$

This definition allows us to write the matrices that generate the unpaired trap and paired trap blocks in the compact forms

$$\hat{U}_{k,j,i} = \begin{pmatrix} 0 & & & \\ & 0_{2 \times 2} & & \\ & & \hat{s}_k \otimes \hat{s}_j \otimes \hat{s}_i & \\ & & & 0_{4 \times 4} \end{pmatrix}, \quad (13)$$

and

$$\hat{T}_{j,i} = \begin{pmatrix} 0 & & & \\ & 0_{2 \times 2} & & \\ & & 0_{8 \times 8} & \\ & & & \hat{s}_j \otimes \hat{s}_i \end{pmatrix}. \quad (14)$$

According to this scheme the population density of unpaired traps is $\hat{N}_1 = \hat{U}_{0,0,0}$, and the one for paired traps is $\hat{N}_2 = \hat{T}_{0,0}$. Similarly, the CB electrons' spin operators are: $\hat{S}_x = \hat{S}_1$, $\hat{S}_y = \hat{S}_2$, and $\hat{S}_z = \hat{S}_3$. We have the same case for the bound electron spin operator components in unpaired traps where $\hat{S}_{cx} = \hat{U}_{1,0,0}$, $\hat{S}_{cy} = \hat{U}_{2,0,0}$, and $\hat{S}_{cz} = \hat{U}_{3,0,0}$. The operators of

the nuclear spin of unpaired traps and paired traps can be expressed as linear combinations of the elements of Λ as

$$\hat{I}_1 = \mathcal{M}\hat{U}, \quad (15)$$

$$\hat{I}_2 = \mathcal{M}\hat{T}, \quad (16)$$

where

$$\hat{U}^\top = (\hat{U}_{0,0,1}, \hat{U}_{0,1,1}, \hat{U}_{0,2,2}, \hat{U}_{0,0,2}, \hat{U}_{0,1,2}, \hat{U}_{0,2,1}, \hat{U}_{0,0,3}, \hat{U}_{0,3,0}), \quad (17)$$

$$\hat{T}^\top = (\hat{T}_{0,1}, \hat{T}_{1,1}, \hat{T}_{2,2}, \hat{T}_{0,2}, \hat{T}_{1,2}, \hat{T}_{2,1}, \hat{T}_{0,3}, \hat{T}_{3,0}), \quad (18)$$

and

$$\mathcal{M} = \begin{bmatrix} \sqrt{3} & 2 & 2 & 0 & 0 & 0 & 0 & 0 \\ 0 & 0 & 0 & \sqrt{3} & -2 & 2 & 0 & 0 \\ 0 & 0 & 0 & 0 & 0 & 0 & 1 & 2 \end{bmatrix}. \quad (19)$$

C. Dissipator

The dissipator can be separated into six parts

$$\mathcal{D}(\rho) = \mathcal{G} + \mathcal{D}_{\text{SDR}} + \mathcal{D}_S + \mathcal{D}_{\text{SC}} + \mathcal{D}_1 + \mathcal{D}_2. \quad (20)$$

Here \mathcal{G} contains the terms, which correspond to VB hole and CB electron photogeneration. The selective capture of CB electrons in unpaired traps according to their relative spin orientation and the subsequent recombination to the VB are described by the \mathcal{D}_{SDR} dissipator. CB and bound electron spin relaxations are accounted for by \mathcal{D}_S and \mathcal{D}_{SC} . Nuclear spin relaxation of unpaired traps and paired traps are introduced through the dissipators \mathcal{D}_1 and \mathcal{D}_2 .

The term \mathcal{G} that models the generation of electrons and holes is given by

$$\mathcal{G} = (G_\uparrow + G_\downarrow)(\hat{p} + \hat{n}) + 2(G_\uparrow - G_\downarrow)\hat{e} \cdot \hat{S}, \quad (21)$$

where G_\uparrow and G_\downarrow are the spin-up and spin-down electron generation rates. The unit vector \hat{e} is collinear with the incident light.

To build the \mathcal{D}_{SDR} part of the dissipator we resort to the two-charge model [20,21,27,29] given by the following kinetic equations ($\hbar = 1$)

$$\dot{n} = -c_n(nN_1 - 4\mathbf{S} \cdot \mathbf{S}_c) + G_\uparrow + G_\downarrow, \quad (22)$$

$$\dot{p} = -c_p N_2 p + G_\uparrow + G_\downarrow, \quad (23)$$

$$\dot{N}_1 = -c_n(nN_1 - 4\mathbf{S} \cdot \mathbf{S}_c) + c_p N_2 p, \quad (24)$$

$$\dot{N}_2 = c_n(nN_1 - 4\mathbf{S} \cdot \mathbf{S}_c) - c_p N_2 p. \quad (25)$$

$$\dot{\mathbf{S}} = -c_n(\mathbf{S}N_1 - \mathbf{S}_c n) - \frac{1}{\tau_s} \mathbf{S} + \boldsymbol{\omega} \times \mathbf{S} + \frac{G_\uparrow - G_\downarrow}{2} \hat{e}, \quad (26)$$

$$\dot{\mathbf{S}}_c = -c_n(\mathbf{S}_c n - \mathbf{S}N_1) - \frac{1}{\tau_{sc}} \mathbf{S}_c + \boldsymbol{\Omega} \times \mathbf{S}_c. \quad (27)$$

In the above equations, the population densities of CB electrons and VB holes are given by n and p respectively. The density of unpaired traps is N_1 , N_2 is the density of electron singlets hosted by the centers (paired traps), and consequently $N_c = N_1 + N_2$ is the total density of Ga centers. The vectors \mathbf{S} and \mathbf{S}_c represent the average spin polarizations of free and bound electrons. The spin-dependent capture of free electrons in the Ga centers is ensured by the recombination rate terms $c_n(nN_1 - 4\mathbf{S} \cdot \mathbf{S}_c)$ and $c_n(\mathbf{S}N_1 - \mathbf{S}_c n)$ where c_n is a constant. Notice that these two terms vanish when the system is fully polarized, i.e., $S_z = n/2$, $S_x = S_y = 0$, $S_{cz} = N_1/2$, and $S_{cx} = S_{cy} = 0$. The recombination rate of one of the electrons trapped in the Ga centers to the VB is given by the terms $c_p N_2 p$ where c_p is a constant. We thus require that the dissipator's structure is such that the master equation reduces to Eqs. (22)–(27) when the hyperfine interaction is lifted ($A = 0$). This may be achieved by identifying n , p , N_1 , N_2 , \mathbf{S} , and \mathbf{S}_c with the quantum statistical average of the corresponding operators, namely $n = \text{Tr}[\rho \hat{n}]$, $p = \text{Tr}[\rho \hat{p}]$, $N_1 = \text{Tr}[\rho \hat{N}_1]$, $N_2 = \text{Tr}[\rho \hat{N}_2]$, $\mathbf{S} = \text{Tr}[\rho \hat{\mathbf{S}}]$, and $\mathbf{S}_c = \text{Tr}[\rho \hat{\mathbf{S}}_c]$. As well, the quantum statistical average of any generator of Λ is given by $\lambda_q = \text{Tr}[\rho \hat{\lambda}_q]$ and therefore, the density matrix can be expanded as

$$\rho = \sum_{q=1}^{85} \frac{\text{Tr}[\rho \hat{\lambda}_q]}{\text{Tr}[\hat{\lambda}_q^2]} \hat{\lambda}_q = \sum_{q=1}^{85} \frac{\lambda_q}{\text{Tr}[\hat{\lambda}_q^2]} \hat{\lambda}_q. \quad (28)$$

The SDR part of the dissipator \mathcal{D}_{SDR} can also be expanded in terms of the elements of Λ as

$$\mathcal{D}_{\text{SDR}} = \sum_{q=1}^{85} \frac{C[\hat{\lambda}_q]}{\text{Tr}[\hat{\lambda}_q^2]} \hat{\lambda}_q = \sum_{q=1}^{85} \frac{C_q}{\text{Tr}[\hat{\lambda}_q^2]} \hat{\lambda}_q. \quad (29)$$

To determine the coefficients $C_q \equiv C[\hat{\lambda}_q] = \text{Tr}[\hat{\lambda}_q \mathcal{D}_{\text{SDR}}]$ we insert (29) in the master equation (2) and multiply by \hat{n} , \hat{p} , \hat{N}_1 , \hat{N}_2 , $\hat{\mathbf{S}}$, or $\hat{\mathbf{S}}_c$. By taking the trace of the resulting equation we readily find the coefficients

$$C[\hat{p}] = -c_p p N_2, \quad (30)$$

$$C[\hat{n}] = -c_n(nN_1 - 4\mathbf{S} \cdot \mathbf{S}_c), \quad (31)$$

$$C[\hat{N}_1] = -c_n(nN_1 - 4\mathbf{S} \cdot \mathbf{S}_c) + c_p N_2 p, \quad (32)$$

$$C[\hat{N}_2] = c_n(nN_1 - 4\mathbf{S} \cdot \mathbf{S}_c) - c_p N_2 p, \quad (33)$$

$$C[\hat{\mathbf{S}}] = -c_n(\mathbf{S}N_1 - \mathbf{S}_c n), \quad (34)$$

$$C[\hat{\mathbf{S}}_c] = -c_n(\mathbf{S}_c n - \mathbf{S}N_1). \quad (35)$$

At this point we have considerable freedom since these equations only define 10 of the 85 coefficients needed to fully determine the \mathcal{D}_{SDR} dissipator. However, the choices get narrowed down by imposing the symmetry and invariance properties that the system is expected to satisfy. As the most basic requirement, the master equation must be invariant under any arbitrary rotation in accordance with the space's isotropy. The tensors $\hat{T}_{j,i}$ and $\hat{U}_{k,j,i}$ must therefore transform by the

corresponding laws. The complete set of coefficients is thus given by

$$C[\hat{p}] = -c_p p T_{0,0}, \quad (36)$$

$$C[\hat{n}] = -c_n \left(S_0 U_{0,0,0} - 4 \sum_{r=1}^3 S_r U_{r,0,0} \right), \quad (37)$$

$$C[\hat{S}_k] = -c_n (S_k U_{0,0,0} - S_0 U_{k,0,0}), \quad (38)$$

$$C[\hat{U}_{0,j,i}] = c_p p T_{j,i} - c_n \left(S_0 U_{0,j,i} - 4 \sum_{r=1}^3 S_r U_{r,j,i} \right), \quad (39)$$

$$C[\hat{U}_{k,j,i}] = -c_n (S_0 U_{k,j,i} - S_k U_{0,j,i}), \quad (40)$$

$$C[\hat{T}_{j,i}] = -c_p p T_{j,i} + c_n \left(S_0 U_{0,j,i} - 4 \sum_{r=1}^3 S_r U_{r,j,i} \right), \quad (41)$$

where $i, j = 0, 1, 2, 3$ and $k = 1, 2, 3$. The spin precession terms $\boldsymbol{\omega} \times \mathbf{S}$ and $\boldsymbol{\Omega} \times \mathbf{S}_c$, absent in Eqs. (36)–(41), are accounted for by the Zeeman terms in the Hamiltonian (3) since they concern the coherent evolution of the system.

The SDR part of the dissipator also excludes the spin relaxation of CB and bound electrons. These terms enter the dissipator through \mathcal{D}_S and \mathcal{D}_{SC} as

$$\mathcal{D}_S = -\frac{1}{\tau_s} \sum_{q=3}^5 \frac{\lambda_q}{\text{Tr}[\lambda_q^2]} \hat{\lambda}_q = -\frac{2}{\tau_s} \sum_{i=1}^3 S_i \hat{S}_i, \quad (42)$$

$$\mathcal{D}_{SC} = -\frac{1}{\tau_{sc}} \sum_{k=1}^3 \sum_{j,i=0}^3 \frac{U_{k,j,i}}{\text{Tr}[\hat{U}_{k,j,i}^2]} \hat{U}_{k,j,i}. \quad (43)$$

The CB electron spin relaxation time due to the Dyakonov-Perel mechanism is given by τ_s , while τ_{sc} is the phenomenological bound electron spin relaxation time in Ga centers [36,37]. The dissipators (42) and (43) yield the CB and bound electron spin relaxation terms \mathbf{S}/τ_s and \mathbf{S}_c/τ_{sc} in the two-charge model.

D. Nuclear spin relaxation

To get an insight into the role of the possible mechanisms involved in nuclear spin relaxation we consider three different models: nonselective, dipolar, and quadrupolar. As a reference we also study the effects in the absence of spin relaxation. The dipolar and quadrupolar interactions are dealt through the Wangsness, Bloch, and Redfield relaxation theory [40–43] summarized in Appendix A.

First, we study the nonselective [37] dissipators for unpaired traps and paired traps given by

$$(\mathcal{D}_1)_{sm,s'm'} = -\frac{1}{\tau_{n1}} \left(\rho_{1;s,m;s',m'} - \frac{\delta_{m,m'}}{4} \sum_{m''=-3/2}^{3/2} \rho_{1;s,m'';s',m''} \right), \quad (44)$$

$$(\mathcal{D}_2)_{m,m'} = -\frac{1}{\tau_{n2}} \left(\rho_{2;m,m'} - \frac{\delta_{m,m'}}{4} \sum_{m''=-3/2}^{3/2} \rho_{2;m'',m''} \right), \quad (45)$$

where $s = -1/2, 1/2$ and $m = -3/2, -1/2, 1/2, 3/2$ are the bound electron spin and nuclear spin indices. This dissipator is highly symmetrical.

Second, we consider the relaxation due to the dipolar interactions between neighboring Ga nuclei. In this case, the Hamiltonian (A1) only contains the irreducible spherical tensors of rank $k = 1$. The terms in this Hamiltonian correspond to the angular momentum operators interacting with a random local field. Substituting (A6) and (A7) in (A5) we obtain the dissipators for unpaired traps and paired traps in the form

$$\mathcal{D}_1 = -\frac{1}{3\tau_{n1}} \sum_{i=1}^3 [\hat{I}_{1i}, [\hat{I}_{1i}, \rho]], \quad (46)$$

$$\mathcal{D}_2 = -\frac{1}{3\tau_{n2}} \sum_{i=1}^3 [\hat{I}_{2i}, [\hat{I}_{2i}, \rho]], \quad (47)$$

where \hat{I}_{1i} and \hat{I}_{2i} are the i th components of the nuclear spin operators for unpaired traps and paired traps, respectively. The nuclear spin relaxation times for unpaired and paired traps are considered to be different in principle and therefore are set to τ_{n1} and τ_{n2} .

Finally, we study the relaxation due to the quadrupole interaction with random fluctuation of the local electric field gradient. The Hamiltonian takes the form of (A1) where $k = 2$. The substitution of the irreducible spherical tensors of the rank $k = 2$ defined by Eqs. (A8)–(A10) in terms of the nuclear angular momentum components (A5) leads to the following dissipators

$$\mathcal{D}_1 = -\frac{1}{2\tau_{n1}} \sum_{i=1}^5 [\hat{Q}_{1i}, [\hat{Q}_{1i}, \rho]], \quad (48)$$

$$\mathcal{D}_2 = -\frac{1}{2\tau_{n2}} \sum_{i=1}^5 [\hat{Q}_{2i}, [\hat{Q}_{2i}, \rho]]. \quad (49)$$

Here, the operators \hat{Q}_{1i} and \hat{Q}_{2i} are related to the rank $k = 2$ irreducible spherical tensors and therefore can be expressed in terms of the nuclear spin operators as

$$\hat{Q}_{n,1} = \frac{1}{2\sqrt{3}} (\hat{I}_{nx}^2 - \hat{I}_{ny}^2), \quad (50)$$

$$\hat{Q}_{n,2} = \frac{1}{2\sqrt{3}} (\hat{I}_{nx} \hat{I}_{ny} + \hat{I}_{ny} \hat{I}_{nx}), \quad (51)$$

$$\hat{Q}_{n,3} = \frac{1}{2\sqrt{3}} (\hat{I}_{nx} \hat{I}_{nz} + \hat{I}_{nz} \hat{I}_{nx}), \quad (52)$$

$$\hat{Q}_{n,4} = \frac{1}{2\sqrt{3}} (\hat{I}_{ny} \hat{I}_{nz} + \hat{I}_{nz} \hat{I}_{ny}), \quad (53)$$

$$\hat{Q}_{n,5} = \frac{1}{6} (2\hat{I}_{nz}^2 - \hat{I}_{ny}^2 - \hat{I}_{nx}^2). \quad (54)$$

The explicit forms of the dissipators corresponding to the dipolar interaction (46)–(47) and quadrupole interaction (48)–(49) are presented in Appendix B.

III. RESULTS AND DISCUSSION

The model developed above is used in this section to examine the interplay of the hyperfine interaction and the

nuclear spin relaxation mechanisms in the continuous wave and pulsed excitation regimes. First, the theoretical results are compared with previous experimental observations under continuous wave excitation in order to identify the main interaction behind nuclear spin relaxation and hyperfine interaction in Ga centers. Then, we analyze spin dynamics of the bound electrons and nuclei in the pulsed excitation regime. We outline a method for detecting the bound electron and nuclear spin coherent oscillations induced by hyperfine interaction by means of a pump-probe PL scheme.

In order to extract information from the model, we start by building the system of kinetic equations that follow from the master equation (2). By multiplying both sides of Eq. (2) by $\hat{\lambda}_q$, inserting the density matrix in the form (28) into the resulting expression and taking the trace we obtain a set of $n = 85$ differential equations of the form

$$\begin{aligned} \dot{\lambda}_q &= \frac{i}{\hbar} \text{Tr}[[H, \hat{\lambda}_q] \rho] + \text{Tr}[\mathcal{D} \hat{\lambda}_q] \\ &= F_q(\lambda_1, \lambda_2, \dots, \lambda_n, t), \quad q = 1, 2, \dots, n. \end{aligned} \quad (55)$$

Unlike the two-charge model that only considers the SDR mechanism, Zeeman interaction, and electron spin relaxation, these new kinetic equations also take into account the hyperfine interaction and nuclear spin relaxation.

We study the spin dynamics of electrons and nuclei by numerically solving the system of ordinary differential equations (55). The relevant parameters are then extracted from the thus obtained λ_q functions, which in turn are the quantum statistical averages. We assume that before the optical excitation ($t = 0$) the unpaired traps are equally populated and that the electrons as well as the nuclei are completely unpolarized. Therefore, initially $N_1(0) = \lambda_6(0) = N_c$ and $\lambda_q = 0$ for $q \neq 6$. Notice that these initial conditions also imply that at this stage there are no paired traps, namely $N_2(0) = \lambda_{70}(0) = 0$.

A. Nuclear spin relaxation: Continuous wave regime

Under continuous wave stimulation, the generation of spin up and spin down electrons is given by the smooth step function

$$G_{\uparrow\downarrow} = WG \frac{1 \pm P_i}{4} \left[1 + \tanh \left(\frac{t - t_0}{\sigma} \right) \right], \quad (56)$$

where W is the excitation power, $G = 2.3 \times 10^{23} \text{ mW}^{-1} \text{ s}^{-1} \text{ cm}^{-3}$ is the power to generated electron ratio, $P_i = \pm 0.15$ is the spin polarization degree of the optically generated CB electrons, $t_0 = 100 \text{ ps}$ is the onset time of the excitation and $\sigma = 10 \text{ ps}$ is the duration of the onset. The system is allowed to evolve for a sufficiently long time (200 ns) to reach steady-state conditions.

Some of other parameters as $N_c = 3 \times 10^{15} \text{ cm}^{-3}$, $\tau_s = 110 \text{ ps}$, $\tau_{sc} = 1700 \text{ ps}$, $\tau^* = 1/c_n N_c = 4.4 \text{ ps}$, $\tau_h^* = 1/c_p N_c = 12 \text{ ps}$, $g = +1$, and $g_c = +2$ where estimated from previous experimental results [20,21,32,51]. For the nuclei at the Ga centers, the hyperfine parameter was estimated to be $A = 6.9 \times 10^{-2} \text{ cm}^{-1} = 8.5 \mu\text{eV}$, the average hyperfine parameter of the two stable isotopes of Ga atoms [22,32,36]. The nuclear spin relaxation times τ_{n1} and τ_{n2} are determined below by comparing the theoretical calculations with the experimental results.

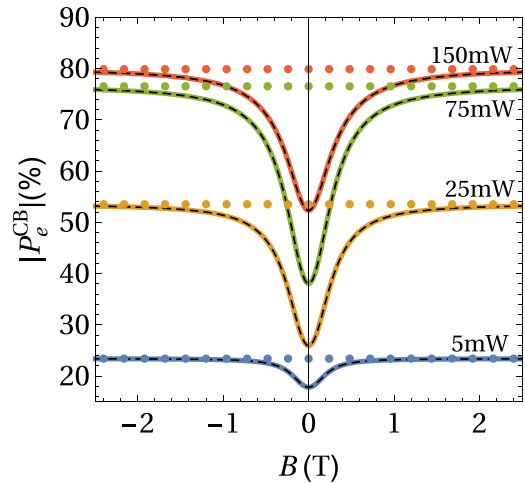


FIG. 2. P_e^{CB} calculated as a function of a magnetic field in the Faraday configuration for different pump powers and nonselective nuclear spin relaxation under σ^+ (solid lines) and σ^- (dashed lines). The nuclear spin relaxation times are $\tau_{n1} = 5405 \text{ ps}$ and $\tau_{n2} = 446 \text{ ps}$. Dotted horizontal lines present the behavior of CB electron polarization in the absence of nuclear spin relaxation.

As we stated above, the two key features behind the hyperfine interaction in Ga centers are a growth in the PL intensity J and degree of circular polarization P_e^{CB} [32,34–37] and an Overhauser-like magnetic field [32,33,35–37]. They are observed under circularly polarized excitation and a Faraday configuration magnetic field B_z .

More specifically for the first feature, $P_e^{CB}(B_z)$ and $J(B_z)$ exhibit a minimum shifted from $B_z = 0$. As $|B_z|$ increases, P_e^{CB} and $J(B_z)$ saturate at values above $B_z \approx 25 \text{ mT}$ where Zeeman energies are comparable to the hyperfine interaction. In this region the hyperfine interaction has been completely exceeded by the Zeeman interaction and therefore the bound electrons and nuclei in the Ga centers are effectively decoupled. The degree of circular polarization of the CB to VB photoluminescence as a function of the Faraday configuration magnetic field can be described by an inverted Lorentzian-like curve. In Fig. 2 we have calculated the CB electron spin polarization degree $P_e^{CB} = 2S_z/n$ as a function of the magnetic field in Faraday configuration B_z under a circularly polarized excitation. In this case we have chosen the spin relaxation times $\tau_{n1} = 5405 \text{ ps}$ and $\tau_{n2} = 446 \text{ ps}$ that give good quantitative agreement with the experiment. The $P_e^{CB} = 2S_z/n$ dependence for the nonselective mechanism is shown in Fig. 2 for different pump powers W . As a reference, Fig. 2 also presents the behavior observed in the absence of nuclear spin relaxation ($\mathcal{D}_1 = \mathcal{D}_2 = 0$) as thick dotted lines. These plots show that despite the hyperfine interaction, in the absence of spin relaxation, $P_e^{CB}(B_z)$ does not display any sign of the spin filtering enhancement. These results are exactly the same as those obtained with the two charge model that does not contain the effects of the hyperfine interaction. Therefore, in order for the effects of the hyperfine interaction to be visible, nuclear spin relaxation is essential.

The second experimental feature of this phenomenon is a shift of the minimum of the plots $P_e^{CB}(B_z)$ and $J(B_z)$ with respect to $B_z = 0$ that points to the existence of an

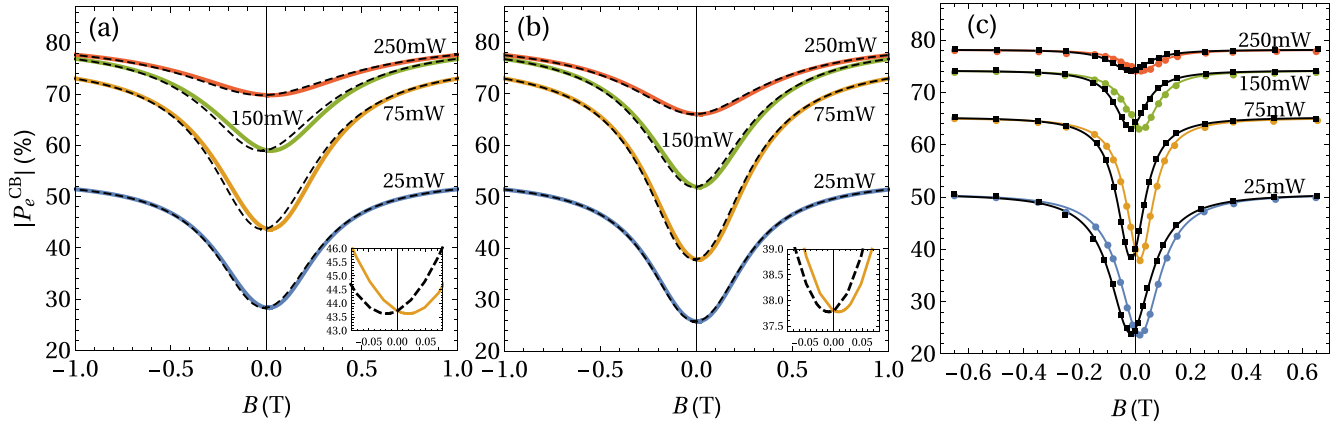


FIG. 3. Conduction band electron spin polarization P_e^{CB} as a function of the magnetic field in the Faraday configuration for pumping power $W = 25, 75, 150,$ and 250 mW. Theoretical results for the (a) dipolar and (b) quadrupolar models under σ^+ (solid lines) and σ^- (dashed lines) light excitation. (c) Experimental results under σ^+ (circles) and σ^- (squares) light excitation [32,37], solid lines are the guides for the eye. The insets in (a) and (b) show the detail of the displacement of the P_e^{CB} curves for σ^+ (solid lines) and σ^- (dashed lines) that is induced by the Overhauser-like magnetic field at $W = 75$ mW.

Overhauser-like magnetic field [33]. The $P_e^{CB}(B_z)$ and $J(B_z)$ curves are shifted to the positive or negative magnetic field depending on the helicity of the circularly polarized exciting light. Thereby, under σ^- and σ^+ excitation the minimum is located at $B_z = B_{\text{eff}} < 0$ and $B_z = B_{\text{eff}} > 0$, respectively. The experimental results show that the Overhauser-like magnetic field B_{eff} grows with the excitation power W until it apparently saturates at approximately 25 mT. The nonselective dissipator yields vanishing B_{eff} as no shift is observed for P_e^{CB} in Fig. 2. This dissipator is too symmetric to be able to produce an Overhauser-like magnetic field and hence must be ruled out as the leading nuclear spin relaxation mechanism.

The dipolar and quadrupolar mechanisms are quite different from the nonselective one. Figures 3 and 4 show the effect of the dipolar and quadrupolar nuclear spin relaxation mechanisms on the CB electron spin polarization $P_e^{CB}(B_z)$ and the PL intensity $J(B_z)$ as functions of the longitudinal magnetic field at different excitation powers. Contrary to the nonselective mechanism, the dipolar and quadrupolar ones

yield nonvanishing B_{eff} as it can be seen in Figs. 3(a)–3(b) and 4(a)–4(b). In Figs. 4(a)–4(b) the PL intensity is calculated as $J(B_z) = c_r n p$ where c_r is the bimolecular recombination rate.

Even though the calculated shifts produced by both mechanisms qualitatively agree with the experimental observations [see Figs. 3(c) and 4(c)], only the dipolar one is able to accurately fit the experimental measurements as we discuss below. In addition to the Overhauser-like magnetic field, two features that strongly depend on the nuclear spin relaxation mechanism are the depths of the inverted Lorentzian-like $P_e^{CB}(B_z)$ and $J(B_z)$ curves, which parametrized by $\xi = P_e^{CB}(\infty)/P_e^{CB}(0)$ and $\zeta = J(\infty)/J(0)$, respectively. To discern which of the two mechanisms is the dominant one, we compare our theoretical calculations with the experimental observations of B_{eff} , ξ , and ζ [32,33,37]. The power dependence of B_{eff} , ξ , and ζ is determined by finding the minima, $P_e^{CB}(0)$ and $J(0)$, and maxima, $P_e^{CB}(\infty)$ and $J(\infty)$, of $P_e^{CB}(B_z)$ and $J(B_z)$ for different excitation powers.

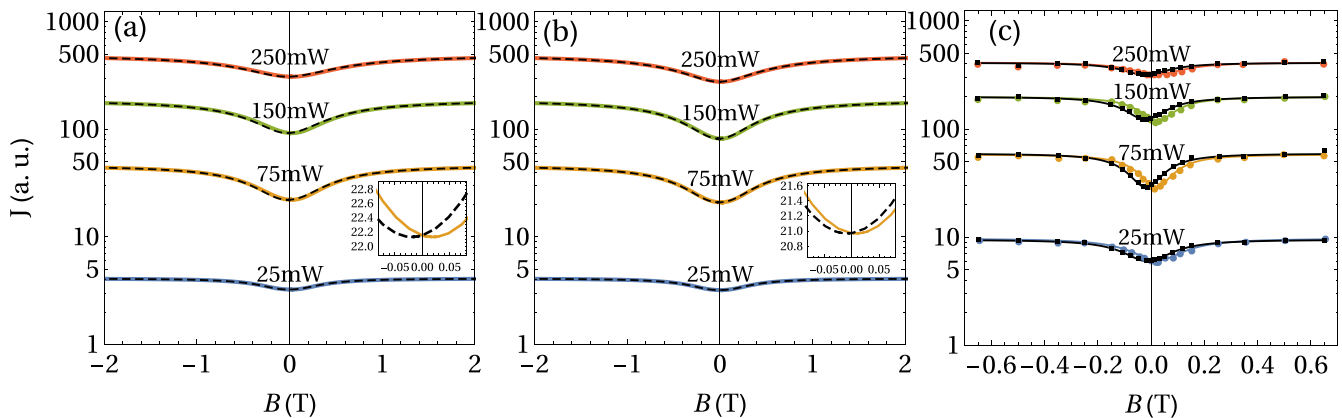


FIG. 4. PL intensity J as a function of the magnetic field in the Faraday configuration for pumping power $W = 25, 75, 150,$ and 250 mW. Theoretical results for the (a) dipolar and (b) quadrupolar models under σ^+ (solid lines) and σ^- (dashed lines) light excitation. (c) Experimental results under σ^+ (circles) and σ^- (squares) light excitation [32,37], solid lines are the guides for the eye. The insets in (a) and (b) show the detail of the displacement of the J curves for σ^+ (solid lines) and σ^- (dashed lines) that is induced by the Overhauser-like magnetic field at $W = 75$ mW.

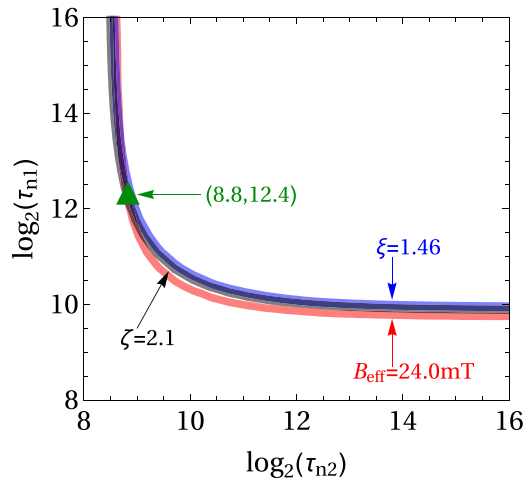


FIG. 5. Isolines of the Overhauser-like magnetic field B_{eff} and depths $\xi = P_e^{CB}(\infty)/P_e^{CB}(0)$ and $\zeta = J(\infty)/J(0)$ at fixed power $W = 120$ mW for the dipolar relaxation mechanism. The isolines for $B_{\text{eff}} = 24$ mT, $\xi = 1.46$ and $\zeta = 2.1$ under an excitation power of $W = 120$ mW are shown. These three lines cross at the point marked with the triangle in $\tau_{n1} = 2^{12.4}$ ps = 5405 ps and $\tau_{n2} = 2^{8.8}$ ps = 446 ps.

In Fig. 5 we plot the isolines for $B_{\text{eff}} = 24$ mT, $\xi = 1.46$, and $\zeta = 2.1$ as functions of the nuclear spin relaxation times τ_{n1} and τ_{n2} . These three correspond to the experimental results observed for an excitation power of $W = 120$ mW [32]. The three isolines intersect at $\tau_{n1} = 5405$ ps and $\tau_{n2} = 446$ ps. In accordance with these results, the B_{eff} , ξ , and ζ isolines at other excitation power coincide at similar τ_{n1} and τ_{n2} values. Collecting the intersecting points of all the experimental results we find that the nuclear spin relaxation times must fall within the ranges 4000 ps $< \tau_{n1} < 9500$ ps and 400 ps $< \tau_{n2} < 700$ ps. The best quantitative agreement with the experimental data is accomplished by using the nuclear spin relaxation times $\tau_{n1} = 5405$ ps and $\tau_{n2} = 446$ ps consistent with the ranges above.

Plots of B_{eff} , ξ , and ζ as functions of the excitation power are shown in Figs. 6(a)–6(d). Whereas Fig. 6(a) shows the magnetic field B_{eff} extracted from the minima of the $\xi(B_z)$ curves, Fig. 6(c) plots the B_{eff} extracted from the $\zeta(B_z)$ minima. It is worth noting that both B_{eff} obtained from the $\xi(B_z)$ and $\zeta(B_z)$ minima yield almost identical experimental and theoretical results. The calculated ξ and ζ as functions of the power present very good quantitative agreement with the experimental data. Likewise, the theoretical values of the Overhauser-like magnetic field B_{eff} remarkably coincide with the experimental results within the range of power values shown in Figs. 6(a) and 6(c). Nevertheless, while the experimental results suggest that B_{eff} as a function of the excitation power saturates at approximately 25 mT, the computed B_{eff} vanishes for powers above 250 mW [not shown in Figs. 6(a) or 6(c)].

Contrary to the dipolar mechanism, the quadrupolar one yields systematically nonintersecting isolines regardless of the excitation power value used to calculate them. In Fig. 7 we present the $B_{\text{eff}} = 24$ mT, $\xi = 1.46$, and $\zeta = 2.1$ isolines that clearly do not intersect. This behavior is observed for all the

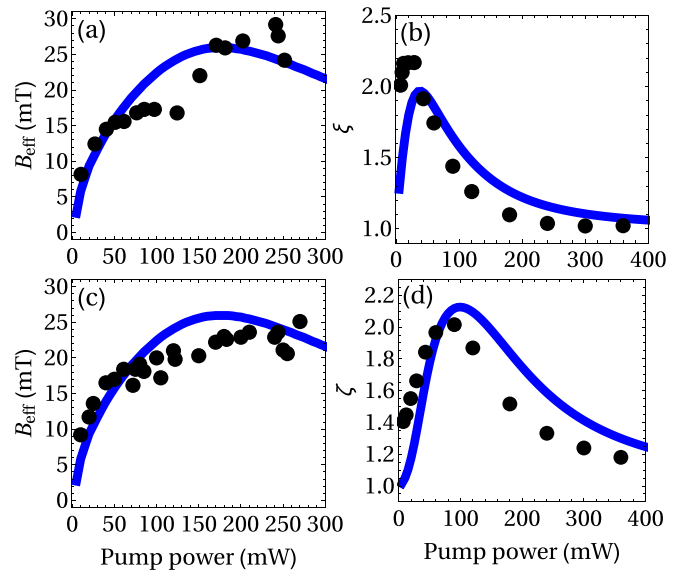


FIG. 6. Overhauser-like magnetic field B_{eff} , ξ , and ζ as functions of the excitation power W for the dipolar nuclear spin relaxation. In (a), the experimental data (circles) present the shift of the free electron polarization dependence $P_e^{CB}(B_z)$ and the simulated curve (line). In (b), shows the experimental (circles) and theoretical (line) results for ξ . The experimental data (circles) in (c) present the shift drawn from the PL intensity dependence $J(B_z)$ and the corresponding theoretical curve (line). In (d), presents the experimental (circles) [32,33,37] and theoretical (line) results for ζ .

excitation powers reported experimentally and therefore we must also rule out the quadrupolar mechanism.

We observe that the calculated widths (≈ 0.3 T) of the inverted Lorentzian curves for either mechanism do not coincide with the experimental ones (≈ 0.2 T). The calculated

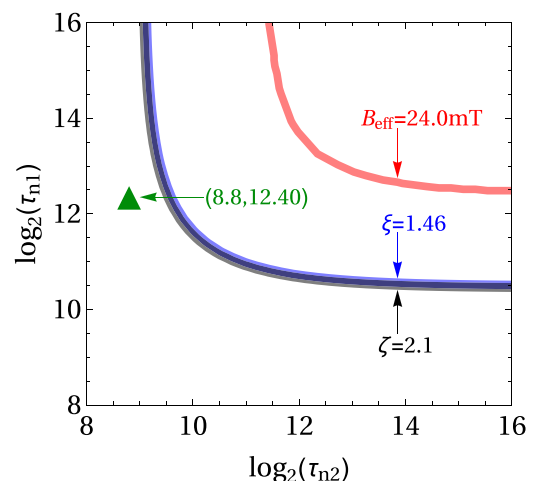


FIG. 7. Isolines of the Overhauser-like magnetic field B_{eff} and depths $\xi = P_e^{CB}(\infty)/P_e^{CB}(0)$ and $\zeta = J(\infty)/J(0)$ at fixed power for the quadrupolar relaxation. The isolines for $B_{\text{eff}} = 24$ mT, $\xi = 1.46$, and $\zeta = 2.1$ under an excitation power of $W = 120$ mW are shown. Even though these three lines do not cross we have marked with a triangle the point $\tau_{n1} = 5405$ ps and $\tau_{n2} = 446$ ps that yield the best fit.

width remains constant for a wide range of parameters and thus it is not related to the nuclear spin relaxation mechanisms. This discrepancy will be discussed elsewhere.

It is important to verify that the nuclear bath is fast enough for the the Redfield theory and the master equation approach to be valid for the dipolar mechanism. The nonperturbed Hamiltonian H_0 contains mainly the hyperfine interaction and the Zeeman energy and therefore $|H_0| = \hbar\omega_0 \approx 10 \mu\text{eV}$. On the other hand, the perturbed Hamiltonian corresponds to the dipolar interaction between neighbouring nuclei and thus $|H_1| \approx \hbar\omega_1 \approx 0.4\text{--}0.6 \text{ peV}$. Equation (A12) then yields

$$\tau_c \ll \omega_1^{-1} \approx 1.14\text{--}1.84 \text{ ms.} \quad (57)$$

The correlation time is obtained from Eq. (A13)

$$\tau_c = \frac{1}{\tau_n \omega_0^2} \approx 1 \text{ ps.} \quad (58)$$

Consequently the time range of validity for the master equation approach in this case is given by

$$1 \text{ ps} \ll t \ll 1 \text{ ms,} \quad (59)$$

in accordance with the results obtained here.

B. Coherent oscillations of electronic and nuclear spins in Ga centers: Pulsed excitation regime

Having identified the nuclear spin relaxation mechanism and the corresponding relaxation times we are in a position to consider time-resolved simulations. Our aim here is to develop a method to observe the coherent oscillations of bound electrons and nuclei in Ga centers. To do so we propose a pump-probe scheme that we describe below.

In pulsed excitation regime, the generation terms are given by

$$G_{\uparrow\downarrow} = \frac{TWG}{\sigma\sqrt{2\pi}} \frac{1 \pm P_i}{2} \left[e^{-\frac{t^2}{2\sigma^2}} + \eta e^{-\frac{(t-\delta t)^2}{2\sigma^2}} \right], \quad (60)$$

where W is the pulse average power, $\sigma = 1 \text{ ps}$ is its width and $T = 12 \text{ ns}$ is the period between repeated pulses [31]. The pump pulse originates at $t = 0$ and the probe is delayed δt .

Figure 8 is an outline of the proposed method. The pump pulse is left circularly polarized and therefore most of the electrons are spin polarized in the $+z$ direction. Likewise, the probe pulses are left circularly polarized Fig. 8 also shows a plot of the bound electron and nuclear spin polarizations as a function of time after being excited by the pump pulse. The pump and probe pulse's widths are exaggerated to make them visible in the given time scale. In this plot it is possible to observe the electron-nucleus flip-flops as oscillations of I_{1z} (dashed lines) and S_{cz} (thick lines) that are phase shifted by $\pi/2$. As indicated in this diagram, the second pulse at time delays t_1 and t_2 probes two extreme situations. In the first one CB electrons and bound electrons are mostly spin polarized in opposite directions. The center is therefore more likely to capture a CB electron whose spin is oriented in the opposite direction to the majority therefore rising the population of electrons in the CB. In contrast, in the second situation centers are more likely to capture electrons whose direction is parallel to the majority diminishing the electron population in the CB.

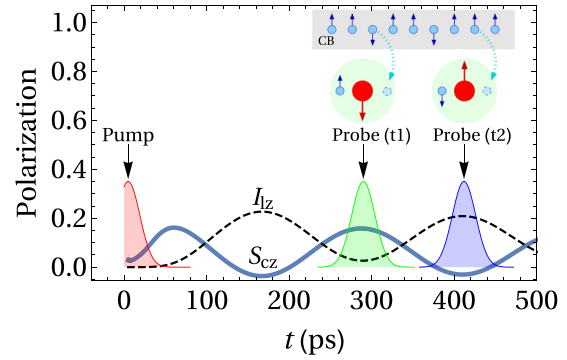


FIG. 8. Time dependence of the spin polarization of bound electrons S_{cz} (solid lines) and nuclei I_{1z} (dashed lines) after being excited by the pump pulse. The pump pulse is left circularly polarized and therefore the majority of the electrons are spin polarized in the $+z$ direction. Two extreme situations are illustrated. In the probe pulse 1 bound electrons are spin polarized in the same direction as CB electrons and in the probe pulse 2 bound electrons are spin polarized in the opposite direction to CB electrons. In the first situation CB electrons with the opposite spin polarization to the majority are rapidly recombined through the Ga centers enhancing the spin filtering effect. In this case a large SDR_r is expected. In contrast, in the second situation, CB electrons whose spin polarization is that of the majority are efficiently recombined lowering the SDR_r .

A good estimate of the electron and hole population in either situation is the time-resolved SDR_r ratio given by

$$SDR_r(t) = \frac{J_-}{J_X} = \frac{n_{\sigma_-}(t)p_{\sigma_-}(t)}{n_{\pi_X}(t)p_{\pi_X}(t)}, \quad (61)$$

where the PL intensity under circularly polarized light $J_- \propto n_{\sigma_-}(t)p_{\sigma_-}(t)$ is proportional to the CB and VB density populations $n_{\sigma_-}(t)$ and $p_{\sigma_-}(t)$. Similarly $J_X \propto n_{\pi_X}(t)p_{\pi_X}(t)$ where $n_{\pi_X}(t)$ and $p_{\pi_X}(t)$ are the density populations of CB electrons and holes under linearly polarized light. If CB electrons are captured spin dependently by the Ga centers then $n_{\sigma_-}(t) > n_{\pi_X}(t)$ and $p_{\sigma_-}(t) > p_{\pi_X}(t)$ and therefore $SDR_r > 1$. In accordance with the above considerations, $SDR_r(\delta t_1) > SDR_r(\delta t) > SDR_r(\delta t_2)$ where $\delta t_1 < \delta t < \delta t_2$. Thus, it is possible to trace the oscillations of bound electrons and

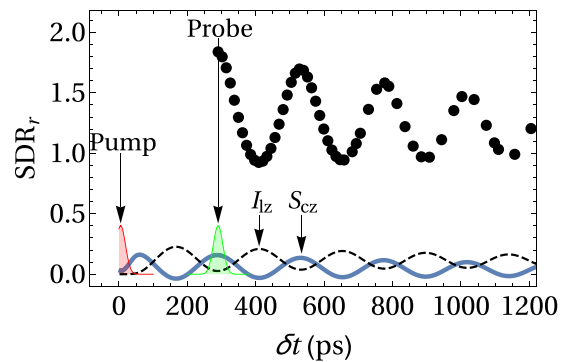


FIG. 9. Trace of the coherent electron-nuclear spin oscillations via the SDR_r . The solid circles correspond to maxima of the time-resolved SDR_r as a function of the time delay δt between the pump and the probe pulses. Below, S_{cz} (solid line) and I_{1z} (dashed line) are presented for reference.

nuclei by successively measuring the time-resolved SDR_r for different probe pulse delays.

By determining the maxima of the time-resolved SDR_r for different probe pulse delays we have obtained the plot displayed in Fig. 9 setting $\eta = 1$. Here the SDR_r maxima are plotted as a function of their corresponding time delays δt as closed circles. Similar results (not shown here) are obtained by calculating the SDR_r from the integrated PL. Below, the spin polarization of bound electrons S_{cz} and nuclear spin polarization I_{1z} are shown for reference. This plot demonstrates that it is possible to trace the coherent oscillations of the spin polarization of bound electrons interacting with the nuclei by means of the time-resolved SDR ratio.

IV. SUMMARY

We have analyzed the spin dynamics of electrons and nuclei in GaAsN by developing a model based on the master equation approach. The main mechanisms behind the spin-dependent recombination are considered as well as the hyperfine interaction in Ga paramagnetic traps. We have demonstrated that the nuclear spin relaxation in centers plays an essential role in reproducing the two most significant signatures of the hyperfine interaction in Ga centers. First, the amplification of the spin filtering effect under a Faraday configuration magnetic field is visible only if some nuclear spin relaxation mechanism is present. Second, the features of the Overhauser-like magnetic field not only depend on the hyperfine interaction but also strongly rely on the nature of the nuclear spin relaxation mechanism. We have tested the dipolar interaction between neighboring Ga atoms and the quadrupolar interaction of Ga centers with random charge distribution background. We have proven that the dipolar is the only mechanism compatible with the experimental observations. Indeed, a scenario where large charge distribution variations are present in the vicinity of the Ga nuclei is difficult to imagine. Although most of the experimental results are correctly reproduced by our model some aspects remain elusive. Two of these are the discrepancies between the saturation values of the Overhauser-like magnetic field B_{eff} in the high-power regime and the widths of the $P_e^{CB}(B_z)$ and $J(B_z)$ curves.

To further explore the effects of the hyperfine interaction and the nuclear spin relaxation we have tested the model in the pulsed excitation regime. In particular, we have proposed a pump-probe scheme that allows us to trace the coherent oscillations of the bound electron spin interacting with its nucleus through the hyperfine interaction.

Even though in principle this model is conceived for Ga centers, it can be easily adapted for other type of centers where dipolar or quadrupolar interactions are the leading mechanisms of nuclear spin relaxation.

ACKNOWLEDGMENTS

French and Russian authors acknowledge funding from LIA CNRS-Ioffe RAS ILNACS. L.A.B. E.L.I. thanks the Russian Foundation for Basic Research (Grants No. 17-02-00383 and No. 17-52-16020). V.K.K. acknowledges the financial support of the Government of Russia (Project No. 14.Z50.31.0021).

This work was partially supported by Programme Investissements d'Avenir under the program ANR-11-IDEX-0002-02, reference ANR-10-LABX-0037-NEXT. A.K. gratefully appreciates the financial support of "Departamento de Ciencias Básicas UAM-A" Grants No. 2232214 and No. 2232215. J.C.S.S. and V.G.I.S. would like to acknowledge the support received from the "Becas de Posgrado UAM" Scholarships No. 2151800745 and No. 2112800069. We are indebted to Professor J. Grabinsky for the careful reading of the manuscript.

APPENDIX A: REDFIELD RELAXATION THEORY

According to the Wangsness, Bloch, and Redfield relaxation theory [40–43] the interaction of a nucleus with its surroundings can be accounted for by the Hamiltonian

$$\mathcal{H}(t) = \gamma \sum_{r=-k}^k f_{k,r}^*(t) \mathbf{T}_{k,r}, \quad (\text{A1})$$

where γ is a constant, $\mathbf{T}_{k,r}$ is a r th component of the rank k irreducible spherical tensor and $f_{k,r}(t)$ is a random function that describes the interaction with the surroundings.

To second order, the average fluctuations of the surroundings with the nucleus are given by the following dissipator

$$\mathcal{D} = -\frac{1}{\hbar^2} \int_{-\infty}^t dt' \overline{[\mathcal{H}(t), [\mathcal{H}(t'), \bar{\rho}]]}, \quad (\text{A2})$$

where $\bar{\rho}$ is the average density matrix. By substituting the Hamiltonian (A1) in (A2) and using the fact that $f_{k,r}^*(t) = (-1)^r f_{k,-r}(t)$ and $\mathbf{T}_{k,r}^\dagger = (-1)^r \mathbf{T}_{k,-r}$ we get the general form of the dissipator

$$\begin{aligned} \mathcal{D} = & -\frac{1}{\hbar^2} \sum_{s,r=-k}^k [\mathbf{T}_{k,s}^\dagger, [\mathbf{T}_{k,r}, \bar{\rho}]] \\ & \times \left(\int_{-\infty}^t dt' \gamma^2 \overline{f_{k,s}(t) f_{k,r}^*(t')} \right). \end{aligned} \quad (\text{A3})$$

The above dissipator describes the interaction of a nucleus with the fluctuations of a random electromagnetic field. The functions $f_{k,s}(t)$ and $f_{k,r}^*(t')$ satisfy the relation

$$\gamma^2 \overline{f_{k,s}(t) f_{k,r}^*(t')} = \delta_{s,r} \xi e^{-|t-t'|/\tau_c}, \quad (\text{A4})$$

where $\xi e^{-|t-t'|/\tau_c}$ is a correlation function, τ_c is the correlation time of the fluctuating field and ξ is the correlation amplitude when $t = t'$. With (A4), the dissipator \mathcal{D} (A3) is simplified to

$$\mathcal{D}_{\text{NSR}} = -\frac{1}{2\tau_n} \sum_{r=-k}^k [\mathbf{T}_{k,r}^\dagger, [\mathbf{T}_{k,r}, \bar{\rho}]], \quad (\text{A5})$$

where $\tau_n = \hbar^2/2\xi\tau_c$ is the nuclear spin relaxation time.

In the case of magnetic dipole interactions, only the irreducible spherical tensors of rank $k = 1$ participate in the Hamiltonian (A1). They can be expressed in terms of the nuclear spin components as

$$\mathbf{T}_{1,0} = \hat{I}_z, \quad (\text{A6})$$

$$\mathbf{T}_{1,\pm 1} = \mp \frac{1}{\sqrt{2}} (\hat{I}_x \pm i \hat{I}_y). \quad (\text{A7})$$

In the case of electric quadrupole interaction k is equal to 2 and the components of irreducible spherical tensors of rank 2 are

$$\mathbf{T}_{2,0} = \frac{1}{6}[2\hat{I}_z^2 - \hat{I}_y^2 - \hat{I}_x^2], \quad (\text{A8})$$

$$\mathbf{T}_{2,\pm 1} = \mp \frac{1}{2\sqrt{6}}[\hat{I}_x \hat{I}_z + \hat{I}_z \hat{I}_x \pm i(\hat{I}_y \hat{I}_z + \hat{I}_z \hat{I}_y)], \quad (\text{A9})$$

$$\mathbf{T}_{2,\pm 2} = \frac{1}{2\sqrt{6}}[(\hat{I}_x^2 - \hat{I}_y^2) \pm i(\hat{I}_x \hat{I}_y + \hat{I}_y \hat{I}_x)]. \quad (\text{A10})$$

In order for the Redfield theory and the master equation approach to be applicable the following conditions must be fulfilled: (i) the bath's correlation time τ_c should be sufficiently short to satisfy the inequality

$$\tau_c \omega_1 \ll 1, \quad (\text{A11})$$

and the density matrix should be valid in the time scale t given by

$$\tau_c \ll t \ll \omega_1^{-1}, \quad (\text{A12})$$

where ω_1 is a characteristic frequency of the perturbation Hamiltonian $|H_1|$ [43,52,53]; (ii) furthermore, the relaxation times should be longer than the correlation time

$$\tau_c \ll \tau_n. \quad (\text{A13})$$

The correlation time in the previous expression may be estimated from [54]

$$\tau_c \approx \frac{1}{\tau_n \omega_0^2}, \quad (\text{A14})$$

where $\hbar\omega_0 = |H_0|$ is the characteristic energy of the unperturbed Hamiltonian.

APPENDIX B: EXPLICIT FORM OF THE DIPOLAR AND QUADRUPOLAR INTERACTIONS

The quadrupolar dissipator for paired trap is given explicitly by

$$(\mathcal{D}_2)_{\frac{3}{2},\frac{3}{2}} = -\frac{1}{\tau_{n2}} \left(\rho_{2;\frac{3}{2},\frac{3}{2}} - \frac{\rho_{2;\frac{1}{2},\frac{1}{2}} + \rho_{2;-\frac{1}{2},-\frac{1}{2}}}{2} \right), \quad (\text{B1})$$

$$(\mathcal{D}_2)_{-\frac{3}{2},-\frac{3}{2}} = -\frac{1}{\tau_{n2}} \left(\rho_{2;-\frac{3}{2},-\frac{3}{2}} - \frac{\rho_{2;\frac{1}{2},\frac{1}{2}} + \rho_{2;-\frac{1}{2},-\frac{1}{2}}}{2} \right), \quad (\text{B2})$$

$$(\mathcal{D}_2)_{\frac{1}{2},\frac{1}{2}} = -\frac{1}{\tau_{n2}} \left(\rho_{2;\frac{1}{2},\frac{1}{2}} - \frac{\rho_{2;\frac{3}{2},\frac{3}{2}} + \rho_{2;-\frac{3}{2},-\frac{3}{2}}}{2} \right), \quad (\text{B3})$$

$$(\mathcal{D}_2)_{-\frac{1}{2},-\frac{1}{2}} = -\frac{1}{\tau_{n2}} \left(\rho_{2;-\frac{1}{2},-\frac{1}{2}} - \frac{\rho_{2;\frac{3}{2},\frac{3}{2}} + \rho_{2;-\frac{3}{2},-\frac{3}{2}}}{2} \right), \quad (\text{B4})$$

$$(\mathcal{D}_2)_{\frac{3}{2},\frac{1}{2}} = -\frac{1}{2\tau_{n2}} (3\rho_{2;\frac{3}{2},\frac{1}{2}} - \rho_{2;-\frac{1}{2},-\frac{3}{2}}), \quad (\text{B5})$$

$$(\mathcal{D}_2)_{-\frac{3}{2},-\frac{1}{2}} = -\frac{1}{2\tau_{n2}} (3\rho_{2;-\frac{3}{2},-\frac{1}{2}} - \rho_{2;\frac{1}{2},\frac{3}{2}}), \quad (\text{B6})$$

$$(\mathcal{D}_2)_{-\frac{1}{2},-\frac{3}{2}} = -\frac{1}{2\tau_{n2}} (3\rho_{2;-\frac{1}{2},-\frac{3}{2}} - \rho_{2;\frac{3}{2},\frac{1}{2}}), \quad (\text{B7})$$

$$(\mathcal{D}_2)_{\frac{1}{2},\frac{3}{2}} = -\frac{1}{2\tau_{n2}} (3\rho_{2;\frac{1}{2},\frac{3}{2}} - \rho_{2;-\frac{3}{2},-\frac{1}{2}}), \quad (\text{B8})$$

$$(\mathcal{D}_2)_{\frac{1}{2},-\frac{1}{2}} = -\frac{1}{\tau_{n2}} \rho_{2;\frac{1}{2},-\frac{1}{2}}, \quad (\text{B9})$$

$$(\mathcal{D}_2)_{-\frac{1}{2},\frac{1}{2}} = -\frac{1}{\tau_{n2}} \rho_{2;-\frac{1}{2},\frac{1}{2}}, \quad (\text{B10})$$

$$(\mathcal{D}_2)_{\frac{3}{2},-\frac{1}{2}} = -\frac{1}{2\tau_{n2}} (3\rho_{2;\frac{3}{2},-\frac{1}{2}} + \rho_{2;\frac{1}{2},-\frac{3}{2}}), \quad (\text{B11})$$

$$(\mathcal{D}_2)_{\frac{1}{2},-\frac{3}{2}} = -\frac{1}{2\tau_{n2}} (3\rho_{2;\frac{1}{2},-\frac{3}{2}} + \rho_{2;\frac{3}{2},-\frac{1}{2}}), \quad (\text{B12})$$

$$(\mathcal{D}_2)_{-\frac{3}{2},\frac{1}{2}} = -\frac{1}{2\tau_{n2}} (3\rho_{2;-\frac{3}{2},\frac{1}{2}} + \rho_{2;-\frac{1}{2},\frac{3}{2}}), \quad (\text{B13})$$

$$(\mathcal{D}_2)_{-\frac{1}{2},\frac{3}{2}} = -\frac{1}{2\tau_{n2}} (3\rho_{2;-\frac{1}{2},\frac{3}{2}} + \rho_{2;-\frac{3}{2},\frac{1}{2}}), \quad (\text{B14})$$

$$(\mathcal{D}_2)_{\frac{3}{2},-\frac{3}{2}} = -\frac{1}{\tau_{n2}} \rho_{2;\frac{3}{2},-\frac{3}{2}}, \quad (\text{B15})$$

$$(\mathcal{D}_2)_{-\frac{3}{2},\frac{3}{2}} = -\frac{1}{\tau_{n2}} \rho_{2;-\frac{3}{2},\frac{3}{2}}. \quad (\text{B16})$$

In a short form the above equations can be presented as

$$(\mathcal{D}_2)_{m,m'} = -\frac{1}{\tau_{n2}} \sum_{m_1,m'_1} \mathcal{Q}_{m,m';m_1,m'_1}^{\text{(EQ)}} \rho_{2;m_1,m'_1}.$$

Then the quadrupolar dissipator for unpaired trap is given by

$$(\mathcal{D}_1)_{s,m;s',m'} = -\frac{1}{\tau_{n1}} \sum_{m_1,m'_1} \mathcal{Q}_{m,m';m_1,m'_1}^{\text{(EQ)}} \rho_{1;s,m_1;s',m'_1}.$$

The dipolar dissipator for paired traps is given explicitly by

$$(\mathcal{D}_2)_{\frac{3}{2},\frac{3}{2}} = -\frac{1}{\tau_{n2}} (\rho_{2;\frac{3}{2},\frac{3}{2}} - \rho_{2;\frac{1}{2},\frac{1}{2}}), \quad (\text{B17})$$

$$(\mathcal{D}_2)_{-\frac{3}{2},-\frac{3}{2}} = -\frac{1}{\tau_{n2}} (\rho_{2;-\frac{3}{2},-\frac{3}{2}} - \rho_{2;-\frac{1}{2},-\frac{1}{2}}), \quad (\text{B18})$$

$$(\mathcal{D}_2)_{\frac{1}{2},\frac{1}{2}} = -\frac{1}{3\tau_{n2}} (7\rho_{2;\frac{1}{2},\frac{1}{2}} - 3\rho_{2;\frac{3}{2},\frac{3}{2}} - 4\rho_{2;-\frac{1}{2},-\frac{1}{2}}), \quad (\text{B19})$$

$$(\mathcal{D}_2)_{-\frac{1}{2},-\frac{1}{2}} = -\frac{1}{3\tau_{n2}} (7\rho_{2;-\frac{1}{2},-\frac{1}{2}} - 3\rho_{2;-\frac{3}{2},-\frac{3}{2}} - 4\rho_{2;\frac{1}{2},\frac{1}{2}}), \quad (\text{B20})$$

$$(\mathcal{D}_2)_{\frac{3}{2},\frac{1}{2}} = -\frac{2}{3\tau_{n2}} (3\rho_{2;\frac{3}{2},\frac{1}{2}} - \sqrt{3}\rho_{2;\frac{1}{2},-\frac{1}{2}}), \quad (\text{B21})$$

$$(\mathcal{D}_2)_{\frac{1}{2},-\frac{1}{2}} = -\frac{2}{3\tau_{n2}} [4\rho_{2;\frac{1}{2},-\frac{1}{2}} - \sqrt{3}(\rho_{2;\frac{3}{2},\frac{1}{2}} + \rho_{2;-\frac{1}{2},-\frac{3}{2}})], \quad (\text{B22})$$

$$(\mathcal{D}_2)_{-\frac{1}{2},-\frac{3}{2}} = -\frac{2}{3\tau_{n2}} (3\rho_{2;-\frac{1}{2},-\frac{3}{2}} - \sqrt{3}\rho_{2;\frac{1}{2},-\frac{1}{2}}), \quad (\text{B23})$$

$$(\mathcal{D}_2)_{\frac{1}{2},\frac{3}{2}} = -\frac{2}{3\tau_{n2}} (3\rho_{2;\frac{1}{2},\frac{3}{2}} - \sqrt{3}\rho_{2;-\frac{1}{2},\frac{1}{2}}), \quad (\text{B24})$$

$$(\mathcal{D}_2)_{-\frac{1}{2},\frac{1}{2}} = -\frac{2}{3\tau_{n2}} [4\rho_{2;-\frac{1}{2},\frac{1}{2}} - \sqrt{3}(\rho_{2;\frac{1}{2},\frac{3}{2}} + \rho_{2;-\frac{3}{2},-\frac{1}{2}})], \quad (\text{B25})$$

$$(\mathcal{D}_2)_{-\frac{3}{2}, -\frac{1}{2}} = -\frac{2}{3\tau_{n2}}(3\rho_{2;-\frac{3}{2}, -\frac{1}{2}} - \sqrt{3}\rho_{2;-\frac{1}{2}, \frac{1}{2}}), \quad (\text{B26})$$

$$(\mathcal{D}_2)_{\frac{3}{2}, -\frac{1}{2}} = -\frac{1}{\tau_{n2}}(3\rho_{2;\frac{3}{2}, -\frac{1}{2}} - \rho_{2;\frac{1}{2}, -\frac{3}{2}}), \quad (\text{B27})$$

$$(\mathcal{D}_2)_{\frac{1}{2}, -\frac{3}{2}} = -\frac{1}{\tau_{n2}}(3\rho_{2;\frac{1}{2}, -\frac{3}{2}} - \rho_{2;\frac{3}{2}, -\frac{1}{2}}), \quad (\text{B28})$$

$$(\mathcal{D}_2)_{-\frac{3}{2}, \frac{1}{2}} = -\frac{1}{\tau_{n2}}(3\rho_{2;-\frac{3}{2}, \frac{1}{2}} - \rho_{2;-\frac{1}{2}, \frac{3}{2}}), \quad (\text{B29})$$

$$(\mathcal{D}_2)_{-\frac{1}{2}, \frac{3}{2}} = -\frac{1}{\tau_{n2}}(3\rho_{2;-\frac{1}{2}, \frac{3}{2}} - \rho_{2;-\frac{3}{2}, \frac{1}{2}}), \quad (\text{B30})$$

$$(\mathcal{D}_2)_{\frac{3}{2}, -\frac{3}{2}} = -\frac{4}{\tau_{n2}}\rho_{2;\frac{3}{2}, -\frac{3}{2}}, \quad (\text{B31})$$

$$(\mathcal{D}_2)_{-\frac{3}{2}, \frac{3}{2}} = -\frac{4}{\tau_{n2}}\rho_{2;-\frac{3}{2}, \frac{3}{2}}. \quad (\text{B32})$$

If the above equations are presented as

$$(\mathcal{D}_2)_{m,m'} = -\frac{1}{\tau_{n2}} \sum_{m_1, m'_1} Q_{m,m';m_1, m'_1}^{(\text{MD})} \rho_{2;m_1, m'_1},$$

then the dipolar dissipator for unpaired trap is given by

$$(\mathcal{D}_1)_{s,m;s',m'} = -\frac{1}{\tau_{n1}} \sum_{m_1, m'_1} Q_{m,m';m_1, m'_1}^{(\text{MD})} \rho_{1;s, m_1; s', m'_1}.$$

-
- [1] A. Auer and G. Burkard, *Phys. Rev. B* **93**, 035402 (2016).
- [2] T. van der Sar, Z. H. Wang, M. S. Blok, H. Bernien, T. H. Taminiu, D. M. Toyli, D. A. Lidar, D. D. Awschalom, R. Hanson, and V. V. Dobrovitski, *Nature (London)* **484**, 82 (2012).
- [3] N. Mizuochi, P. Neumann, F. Rempp, J. Beck, V. Jacques, P. Siyushev, K. Nakamura, D. J. Twitchen, H. Watanabe, S. Yamasaki, F. Jelezko, and J. Wrachtrup, *Phys. Rev. B* **80**, 041201 (2009).
- [4] J. R. Maze, J. M. Taylor, and M. D. Lukin, *Phys. Rev. B* **78**, 094303 (2008).
- [5] J. J. Pla, F. A. Mohiyaddin, K. Y. Tan, J. P. Dehollain, R. Rahman, G. Klimeck, D. N. Jamieson, A. S. Dzurak, and A. Morello, *Phys. Rev. Lett.* **113**, 246801 (2014).
- [6] B. E. Kane, *Nature (London)* **393**, 133 (1998).
- [7] J. J. Pla, K. Y. Tan, J. P. Dehollain, W. H. Lim, J. J. L. Morton, D. N. Jamieson, A. S. Dzurak, and A. Morello, *Nature (London)* **489**, 541 (2012).
- [8] T. D. Ladd, D. Maryenko, Y. Yamamoto, E. Abe, and K. M. Itoh, *Phys. Rev. B* **71**, 014401 (2005).
- [9] A. Laucht, R. Kalra, J. T. Muhonen, J. P. Dehollain, F. A. Mohiyaddin, F. Hudson, J. C. McCallum, D. N. Jamieson, A. S. Dzurak, and A. Morello, *Appl. Phys. Lett.* **104**, 092115 (2014).
- [10] W. Yao, R.-B. Liu, and L. J. Sham, *Phys. Rev. B* **74**, 195301 (2006).
- [11] V. Ivády, K. Szász, A. L. Falk, P. V. Klimov, D. J. Christle, E. Janzén, I. A. Abrikosov, D. D. Awschalom, and A. Gali, *Phys. Rev. B* **92**, 115206 (2015).
- [12] T. D. Ladd, F. Jelezko, R. Laflamme, Y. Nakamura, C. Monroe, and J. L. O'Brien, *Nature (London)* **464**, 45 (2010).
- [13] J. Wrachtrup, S. Yang, and D. D. B. Rao, SPIE Newsroom (2016).
- [14] W. M. Witzel, M. S. Carroll, A. Morello, L. Cywiński, and S. Das Sarma, *Phys. Rev. Lett.* **105**, 187602 (2010).
- [15] R. Hanson, V. V. Dobrovitski, A. E. Feiguin, O. Gywat, and D. D. Awschalom, *Science* **320**, 352 (2008).
- [16] D. Simin, V. A. Soltamov, A. V. Poshakinskiy, A. N. Anisimov, R. A. Babunts, D. O. Tolmachev, E. N. Mokhov, M. Trupke, S. A. Tarasenko, A. Sperlich, P. G. Baranov, V. Dyakonov, and G. V. Astakhov, *Phys. Rev. X* **6**, 031014 (2016).
- [17] J. J. Pla, K. Y. Tan, J. P. Dehollain, W. H. Lim, J. J. L. Morton, F. A. Zwanenburg, D. N. Jamieson, A. S. Dzurak, and A. Morello, *Nature (London)* **496**, 334 (2013).
- [18] P.-F. Braun, X. Marie, L. Lombez, B. Urbaszek, T. Amand, P. Renucci, V. K. Kalevich, K. V. Kavokin, O. Krebs, P. Voisin, and Y. Masumoto, *Phys. Rev. Lett.* **94**, 116601 (2005).
- [19] E. Abe, A. M. Tyryshkin, S. Tojo, J. J. L. Morton, W. M. Witzel, A. Fujimoto, J. W. Ager, E. E. Haller, J. Isoya, S. A. Lyon, M. L. W. Thewalt, and K. M. Itoh, *Phys. Rev. B* **82**, 121201 (2010).
- [20] V. K. Kalevich, E. L. Ivchenko, M. M. Afanasiev, A. Y. Shiryayev, A. Y. Egorov, V. M. Ustinov, B. Pal, and Y. Masumoto, *JETP Lett.* **82**, 455 (2005).
- [21] V. K. Kalevich, A. Y. Shiryayev, E. L. Ivchenko, A. Y. Egorov, L. Lombez, D. Lagarde, X. Marie, and T. Amand, *JETP Lett.* **85**, 174 (2007).
- [22] X. J. Wang, Y. Puttison, C. W. Tu, A. J. Ptak, V. K. Kalevich, A. Y. Egorov, L. Geelhaar, H. Riechert, W. M. Chen, and I. A. Buyanova, *Appl. Phys. Lett.* **95**, 241904 (2009).
- [23] H. M. Zhao, L. Lombez, B. L. Liu, B. Q. Sun, Q. K. Xue, D. M. Chen, and X. Marie, *Appl. Phys. Lett.* **95**, 041911 (2009).
- [24] F. Zhao, A. Balocchi, A. Kunold, J. Carrey, H. Carrre, T. Amand, N. Ben Abdallah, J. C. Harmand, and X. Marie, *Appl. Phys. Lett.* **95**, 241104 (2009).
- [25] F. Zhao, A. Balocchi, G. Truong, T. Amand, X. Marie, X. J. Wang, I. A. Buyanova, W. M. Chen, and J. C. Harmand, *J. Phys.: Condens. Matter* **21**, 174211 (2009).
- [26] Y. Puttison, X. J. Wang, I. A. Buyanova, H. Carrre, F. Zhao, A. Balocchi, X. Marie, C. W. Tu, and W. M. Chen, *Appl. Phys. Lett.* **96**, 052104 (2010).
- [27] E. L. Ivchenko, V. K. Kalevich, A. Y. Shiryayev, M. M. Afanasiev, and Y. Masumoto, *J. Phys.: Condens. Matter* **22**, 465804 (2010).
- [28] D. Paget, *Phys. Rev. B* **30**, 931 (1984).
- [29] C. Weisbuch and G. Lampel, *Solid State Commun.* **14**, 141 (1974).
- [30] C. T. Nguyen, A. Balocchi, D. Lagarde, T. T. Zhang, H. Carrre, S. Mazzucato, P. Barate, E. Galopin, J. Gierak, E. Bourhis, J. C. Harmand, T. Amand, and X. Marie, *Appl. Phys. Lett.* **103**, 052403 (2013).
- [31] A. Kunold, A. Balocchi, F. Zhao, T. Amand, N. B. Abdallah, J. C. Harmand, and X. Marie, *Phys. Rev. B* **83**, 165202 (2011).
- [32] V. K. Kalevich, M. M. Afanasiev, A. Y. Shiryayev, and A. Y. Egorov, *Phys. Rev. B* **85**, 035205 (2012).
- [33] V. K. Kalevich, M. M. Afanasiev, A. Y. Shiryayev, and A. Y. Egorov, *JETP Lett.* **96**, 567 (2012).
- [34] Y. Puttison, X. J. Wang, I. A. Buyanova, and W. M. Chen, *Phys. Rev. B* **87**, 125202 (2013).

- [35] Y. Puttison, X. J. Wang, I. A. Buyanova, L. Geelhaar, H. Riechert, A. J. Ptak, C. W. Tu, and W. M. Chen, *Nat. Commun.* **4**, 1751 (2013).
- [36] C. Sandoval-Santana, A. Balocchi, T. Amand, J. C. Harmand, A. Kunold, and X. Marie, *Phys. Rev. B* **90**, 115205 (2014).
- [37] E. L. Ivchenko, L. A. Bakaleinikov, and V. K. Kalevich, *Phys. Rev. B* **91**, 205202 (2015).
- [38] E. L. Ivchenko, L. A. Bakaleinikov, M. M. Afanasiev, and V. K. Kalevich, *Phys. Solid State* **58**, 1539 (2016).
- [39] M. Dyakonov and V. Perel, *Sov. J. Exp. Theor. Phys.* **36**, 995 (1973).
- [40] R. K. Wangsness and F. Bloch, *Phys. Rev.* **89**, 728 (1953).
- [41] A. Redfield, in *Advances in Magnetic Resonance*, edited by J. S. Waugh (Academic Press, New York, 1965), Vol. 1, pp. 1–32.
- [42] G. W. Leppelmeier and E. L. Hahn, *Phys. Rev.* **142**, 179 (1966).
- [43] J. Kowalewski and L. Maler, *Nuclear Spin Relaxation in Liquids: Theory, Experiments, and Applications*, Series in Chemical Physics (CRC Press, Boca Raton, 2006), Chap. 4.
- [44] N. A. Sinitsyn, Y. Li, S. A. Crooker, A. Saxena, and D. L. Smith, *Phys. Rev. Lett.* **109**, 166605 (2012).
- [45] D. J. Hilton and C. L. Tang, *Phys. Rev. Lett.* **89**, 146601 (2002).
- [46] V. Kalevich, A. Y. Shiryaev, E. Ivchenko, M. Afanasiev, A. Y. Egorov, V. Ustinov, and Y. Masumoto, *Physica B* **404**, 4929 (2009).
- [47] X. Wang, I. A. Buyanova, F. Zhao, D. Lagarde, A. Balocchi, X. Marie, C. Tu, J. Harmand, and W. Chen, *Nat. Mater.* **8**, 198 (2009).
- [48] M. D'yakonov, V. Perel, V. Berkovits, and V. Safarov, *Sov. J. Exp. Theor. Phys.* **40**, 950 (1975).
- [49] B. Zakharchenya, V. Kalevich, V. Kul'kov, and V. Fleisher, *Sov. Phys. Solid State* **23**, 810 (1981).
- [50] F. Meier and B. P. Zakharchenya, *Optical Orientation* (Elsevier, Amsterdam, 2012), Vol. 8, Chap. 5.
- [51] D. Lagarde, L. Lombez, X. Marie, A. Balocchi, T. Amand, V. K. Kalevich, A. Shiryaev, E. Ivchenko, and A. Egorov, *Phys. Status Solidi A* **204**, 208 (2007).
- [52] A. G. Redfield, *IBM J. Res. Dev.* **1**, 19 (1957).
- [53] H.-P. Breuer and F. Petruccione, *The Theory of Open Quantum Systems* (Oxford University Press on Demand, Oxford, 2002), Chap. 3.
- [54] M. Dyakonov, in *Spin Physics in Semiconductors* (Springer, Berlin, 2008), pp. 1–28.